Hindawi
Geofluids
Volume 2021, Article ID 3645438, 13 pages
https://doi.org/10.1155/2021/3645438

Research Article

A Study of Millisecond Blasting on High Bench at Barun Iron Ore Operation

Pengfei Zhang,[1,2] **Runcai Bai**,[3] **Xue Sun**,[2] **Haoran Li**,[1] **Honglu Fei**,[4] **and Shijie Bao**[4]

[1]*School of Mining, Liaoning Technical University, Fuxin, Liaoning 123000, China*
[2]*School of Energy Engineering, Longdong University, Qingyang, Gansu 745000, China*
[3]*Institute of Technology and Equipment for the Development and Utilization of Mineral Resources, Liaoning Provincial College of Engineering, Liaoning Technical University, Fuxin, Liaoning 123000, China*
[4]*School of Science, Liaoning Technical University, Fuxin, Liaoning 123000, China*

Correspondence should be addressed to Pengfei Zhang; 704626564@qq.com, Runcai Bai; bairuncai@163.com, and Xue Sun; sunxue@163.com

Received 23 August 2021; Revised 16 September 2021; Accepted 26 October 2021; Published 3 December 2021

Academic Editor: Richeng Liu

To improve the productivity and efficient of modern large-scale open-cut mines, a number of technologies are developed and trialed, including new blasting equipment, larger blasting holes, high benches, air spacing, and short-delay blasting within holes. However, the relative blasting parameters need field calibration and further investigation of theories on these techniques are required. This paper studied the open-cut bench blasting at Barun Eboxi Mine of Baotou Iron and Steel Group via theoretical analysis on shock wave, numerical simulation, and field test. According to the technical conditions of the site, three sets of vertical boreholes at 310 mm diameter were drilled on 24 m high batter; and three sets of air-spaced charges were set up. The digital electronic detonator was used to initiate at millisecond intervals. The study found that under the condition of 24 m high bench, the use of intermediate air interval is beneficial to the rock fragmentation. The delay time within the hole is 3-8 ms. The bottom of the lower explosives and the top of the upper explosives were devised for initiation to optimize the initiation location. The peak effective stress points are 63.6%, 52.2%, and 8.9% higher, respectively. The field test of high-bench intrahole millisecond blasting in Barun Eboxi mine shows that the intrahole millisecond blasting parameters proposed in this study are feasible.

1. Introduction

Millisecond blasting can improve rock fragmentation while reducing vibration from blasting shoving wave. As bench blasting is a complicated engineer practice and there are many factors that can influence the results, only limited studies on the use of delayed detonation to achieve shock wave collision are available [1–3]. Hence, it is critical to investigate the parameters of millisecond blasting in boreholes. Reference [4] studied the influence of charge-up and millisecond time on blasting vibration via observation on shock waves. They suggested that the millisecond time is closely related to amplitude and range of local amplification effect. Reference [5] used laser dynamic caustics to study the dynamic behavior of cracks between different groups of slits in millisecond blasting holes. Results showed that under the millisecond time conditions, stress wave generated by the first blast hole induced tensile stress on the delayed blast hole wall; this helps crack initiation using the same amount of explosives. Reference [6] used Euler algorithm to establish a fully coupled numerical model of free surface air and water under different parameters and different mesh sizes. Comparison between simulation results and empirical formulas showed that the blasting shock wave propagation through different media is significantly different. At the same time, a method of using the "ratio of the explosive radius to the grid size" to determine the grid size was proposed. Reference [7] used conventional TNT explosives to conduct underwater explosion experiments. The peak pressure and specific impulse of the shock wave were considered as indicators to study the

effects of these three factors on the results of the numerical simulation. Subsequently, the mesh size under various explosive levels was determined. A regression model between explosive level and mesh size was also defined. Reference [8] proposed the concept of fine blasting, suggesting to study multidisciplinary blasting theories, blasting digitization, precise numerical simulation, modernization of fine blasting construction, and construction standardization. The study then quantitatively analyzed and finely controlled the release of explosive energy. This in turn provided theoretical support with blasting design and integrated the research of fine blasting with information technology. Reference [9] studied the influence of the initiation position on blasting-induced coal seam fracturing and permeability and analyzed the characteristics of detonation wave propagation, stress field distribution, and crack development at different initiation positions. In conjunction with the results from numerical simulation, it was concluded that simultaneous detonation at two points can expand the range of local fractures while increasing the detonation locations can shorten the detonation time and result in more uniformly distributed fractures.

Reference [10] suggested that the pressure generated by the collision of two opposite detonating waves during the double-point initiation of the hole is greater than the sum of the intensities of the two shock waves by calculating the range of rock blasting fragmentation in different ways. Most of the above literatures (Cai et al.) have studied the effects of blasting vibration waves, shock waves, and detonation waves on cracks and fractures. The investigation of blasting was mainly on mechanisms and experimental analysis of the initiation position in the hole. There is still a lack of relevant research on the stress field distribution and rock breaking mechanism of millisecond initiation in blasting holes on high benches.

Therefore, the detonation wave and shock wave collision can be used to adjust the explosive energy distribution to meet the requirements of different engineering practices by calibrating the parameters of delay time in the hole, the detonation position, and the detonation combination.

In this study, the 24 m bench expansion on the highwall side of Barun Mine was considered a field example. The shock wave empirical formula in literature [6] was used to express the change of shock wave overpressure during the explosion. At the same time, numerical simulation was used to investigate the rock fracturing mechanism from blasting [11–13]. ANSYS software simulated the detonation sequence parameters including middle-interval charged holes and detonation positions of the upper and lower charge packs. This revealed the distribution of the blasting stress field in the rock during the millisecond blasting on the high bench of Barun Mine.

2. Theory of Shock Wave and Millisecond Time Calculation

2.1. Theoretical Analysis on Shock Wave. The structure of the spaced charge in the hole is shown in Figure 1. According to the layered and segmented millisecond delay detonation method adopted in the field, the explosives in area D of

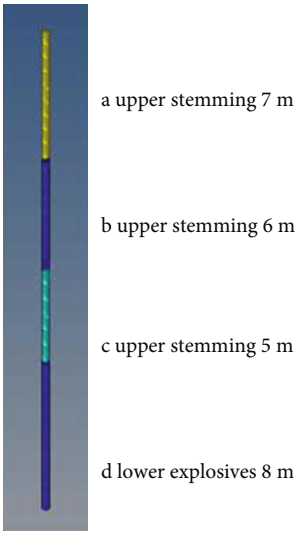

Figure 1: Model charge-up structure: (a) upper stemming; (b) upper explosives; (c) middle air compartment; (d) lower explosives.

Figure 1 detonates first after a millisecond; the detonator at the bottom of area B detonates the explosive after a delay, and the middle section uses air for separation. Under the initiation condition of zone D after t (t = assumed time), the detonation wave front becomes almost flat. Idealistically, the detonation wave will maintain a stable velocity and propagate along the hole. Since t is much smaller than the delay time, the unstable detonation zone generated by one end of the blast hole is much smaller compared to the delay of the entire blast hole. In the calculation, it can be considered that the entire blast hole is still dominated by stable detonation [9]. Based on the conservation law of medium mass between the shock wave front and the explosive air, the equation of the medium motion can be written as

$$\rho_1\left[\frac{\partial_u(R,t)}{\partial t}+\frac{u(R,t)\partial_u(R,t)}{\partial_R}\right]=-\frac{\partial_p(R,t)}{\partial_R},$$
$$\frac{\partial[R_u(R,t)]}{\partial_R}=0, \tag{1}$$
$$\pi\left(R_m^2-R_w^2\right)\rho_0=\pi\left(R^2m-R_{vp}^2\right)\rho_1.$$

At blasting interface, $R=R_{vp}$ and $p=p_{vp}$, such that $2R_{vp}$ $R^*_{vp}+aR^2_{vp}=F(R_{vp})$, where R_w is radius of detonation wave front, R_{vp} is radius of the exploded air, F is function, t is time, ρ_0 is initial density, and ρ_1 is density at any moment. For the closed explosion pressure of the extended charge:

$$p_{vp}=*p_w\left(\frac{R_w}{R_{vp}}\right)^6=\left(\frac{\rho_w D^2}{8}\right)\left(\frac{R_w}{R_{vp}}\right)^6. \tag{2}$$

As exploded air expands, $p_{vp}=2800(R_k/R_{vp})^{4/3}$. When $p_{vp}=p_0$(i.e., $R_{vp}=R_{vd}$), expansion ends, in which p_{vp} is

pressure of exploded air, $*pw$ is average detonation pressure of exploded air, R_w is radius of concentrated charge pack, ρ_w is explosive density, R_{vp} is radius of exploded air, and R_{vd} is blasting cavity radius.

Based on the theoretical analysis of shock wave, the peak pressure of detonation induced shock wave will decrease rapidly with the increase of the blasting center distance. Hence, it can be considered that when the blasting center distance increases to a threshold value, the impact of the shock wave pressure can be ignored. This paper conducted analysis on the change of shock wave peak pressure using the empirical formula of explosion shock wave proposed by Henrych [14]. Results were later compared against numerical calculation. The shock wave peak overpressure is the peak pressure P_f on the shock wave front minus the original pressure in the air P_0 (standard atmospheric pressure). The specific form of Henrych's empirical formula can be written as

$$\begin{gathered}\Delta P_{(t)} = \Delta P_f\left(1 - t/t_p\right)e^{-\alpha 0t/t_p},\\ \Delta P_f = 0.0662/Z + 0.405/Z^2 + 0.3288/Z^3,\\ Z = R/W^{1/3},\\ t_p = 0.001W^{1/3}\left(0.107 + 0.444Z + 0.264Z^2 - 0.129Z^3 + 0.0335Z^4\right),\end{gathered} \tag{3}$$

where ΔP_t is change of shock wave peak overpressure over time, ΔP_f is peak shock wave overpressure, Z is proportional explosion distance, R is the distance between blasting center to the measurement point (1-9 m), W is weight of emulsion explosive (240-250 kg), t_p is the duration of shock wave overexposure, t is the barotropic pressure, and α_0 is the attenuation coefficient.

When explosives are detonated, the medium is the same as the fluid and only longitudinal waves propagate in the medium, such that c_p can be considered close to infinity [15–17]. When $t = 0$, the medium instantly obtains the initial speed and keeps its speed unchanged, and it starts to move, $c_p = (E/\rho_0)/2$ and average pressure $p = Q_w/\Delta V$. ΔV approaches zero while p approaches infinity. Force at this stage can be expressed as $i = p\Delta t$. When the velocity field is considered in conjunction with potential function, it can be assumed that

$$\begin{aligned}u_x &= -\frac{\partial\varphi}{\partial x},\\ u_y &= -\frac{\partial\varphi}{\partial y},\\ u_z &= -\frac{\partial\varphi}{\partial z}.\end{aligned} \tag{4}$$

Under idealistic fluid motion, the continuous functions can be obtained:

$$\begin{aligned}\frac{\partial u_x}{\partial x} + \frac{\partial u_y}{\partial y} + \frac{\partial u_z}{\partial z} &= 0,\\ \frac{\partial^2\varphi}{\partial x^2} + \frac{\partial^2\varphi}{\partial y^2} + \frac{\partial^2\varphi}{\partial z^2} &= 0.\end{aligned} \tag{5}$$

Based on Green's formula [18], the kinetic energy of medium at the point of explosion is equal to the energy of the explosive:

$$Q_w = -\rho_0/2\int\varphi\partial\varphi/\partial n dF. \tag{6}$$

By substituting the spherical velocity field of r into Equation (4),

$$u_r = -\frac{\partial\varphi}{\partial x}C = 4\pi r^2 u_r. \tag{7}$$

By substituting Equation (7) into Equation (6),

$$\begin{aligned}u_x &= -\frac{\partial\varphi}{\partial x},\\ u_y &= -\frac{\partial\varphi}{\partial y},\\ u_z &= -\frac{\partial\varphi}{\partial z},\\ Q_w &== \frac{(r_w Q_w)^{1/2}}{r^2}.\end{aligned} \tag{8}$$

When the energy from explosion is converted to kinetic energy, the medium point starts to move. To better describe the movement process, strain energy (K) was introduced:

$$K = \rho_0 u^2 S \quad A_s = \frac{\sigma^2 s}{2E}. \tag{9}$$

By solving the above equation, the critical velocity can be expressed as

$$u_S = \sigma_s \cdot (\rho_0 E)^{-1/2}. \tag{10}$$

If $K < A_s$, the medium oscillates; otherwise, the medium will experience tensile failure.

2.2. Millisecond Time Calculation. By using theoretical calculation and reasonable selection of the differential interval time,

$$t = \frac{2w}{c_p} + \frac{w}{u_{tr}} + \frac{s}{u_r}. \tag{11}$$

The time to reach the formation of a new free surface can be optimized, so as to obtain the best blasting quality and shock absorption effect. The millisecond time [19] is 25 ms, which is consistent with the actual lagging time between holes. However, it does not explain the whole process of the mutual interference of the stress fields

generated by all the explosive packs. Thereby, this theory is not practical for the calculation of the microdifference in the hole. Pokrovsky [14] proposed that in the microdifference delayed blasting, the decisive factor on the rock fragmentation and the reduction of the seismic effect is the action time of the explosion air pressure ($t = a/c_p + t_{vp}$). This time is about 3~8 ms.

In the formula, t is millisecond time. It is equal to the time required for the formation of a free face, which can be further divided into three parts. The first part is the time required for the stress wave to travel from the center of the explosive pack to the free face and then back to the free face. The second part is the time required to form a crack approximately equal to the minimum chassis resistance line. The third part is the time required for 8-10 mm crack formation. u_{tr} is the speed of crack propagation, s is the crack width, u_r is the average speed of flying rock, a is the interval of explosive packs, and c_p is the speed of longitudinal wave in the medium.

In order to accurately calculate the differential time in the hole, it is based on the research of Zhendong et al. in literature [20].This paper modified the Hanukayev formula from two factors: (i) the formation time of the new free surface and (ii) the residual amount of the stress wave. According to Henry and Jianguo in literature [14], it is assumed that the pressure in the hole at the moment of explosion is p_0, and the moment when the explosion air freely flows out at the beginning, it can be assumed that the higher the pressure, the greater the rate of change, which can be expressed as $p = p(t) = p_0 e^{-\alpha t}$, $p(t)$ is the pressure in the hole, and α is the hypothetical index. The projectile of the rock body from blasting is assumed to be elliptical:

$$\frac{x^2}{a^2} + \frac{y^2}{b^2} = 1, \tag{12}$$

where $a = w \tan(\beta/2)$ and $b = w$.

According to the above formula, the weight of the flying body is $M = \rho_0 V = (\pi/2) H_w 2\rho_0 \tan(\beta/2)$. The pressure acting on the hole element can be therefore calculated as

$$dp = p0e - \alpha t R w \cos\delta d\delta dz. \tag{13}$$

Subsequently, the weight of the flying body can be estimated by integration of the above function. The force can be roughly described by the motion equation of the flying body: $M[d^2 v(t)/dt^2] = P(t)$.

Assume that $p = p_{(t)} = p_0 e^{-\alpha}$ is replaced by a quadratic parabola of $p_{(t)} = mt^2 + nt + 1$. When $p_{(0)} = 1$, $p_{(tm)} = p_m << 1$ and $dp_{(tm)}/dt = 0$. Thus,

$$p(t) = (1 - p_m) t_2/t_2 m + 2(p_m - 1) t/t_m + 1. \tag{14}$$

By combining with the above formula of $P(t)$,

$$v(t) = \frac{(1 - p_m) t^2}{k\alpha^2 t^2 m} + \left[\frac{2(p_m - 1)}{k\alpha^2 t_m} + \frac{1}{k\alpha}\right] t. \tag{15}$$

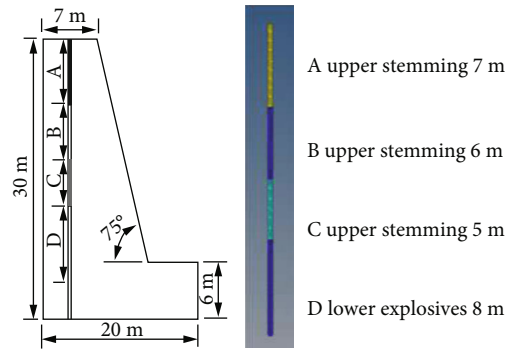

Figure 2: Model charge-up structure.

For $t = t_3$, $v(t_3) = v_p$, $p_0 = 4000\,\text{kg·cm}^{-2}$, and $v_p = 10$ cm. t_3 can be estimated as

$$t_3 = \left[T_3 w^2 \rho_0 \tan(\beta/2)\right]/Ø. \tag{16}$$

The coefficient t_3 in the formula is to consider the influence of some quantities appearing in the equation of motion but not included in the equation. As a first-order approximation, T_3 can be assumed as 80×10^{-6}. Single-row blasting [14] $V_p * = awH$is the blasting volume of a row in the blasting zone; the blasting volume of a single hole can be considered as the average value of the single-row blasting volume. According to Wenhai in literatures[21, 22], the most efficient delay time in the hole-by-hole millisecond blasting is at 25 ms. In summary, the dolomite blasting time within the hole was defined as $t = t_1 + t_2 + t_3 = 3 \sim 8$ ms.

3. Numerical Simulation on Millisecond Blasting and Field Validation

To improve the simulation process, the medium in the model was set as a homogeneous, continuous, and isotropic elastic-plastic material with no initial stress. A symmetrical model was established with the z-axis as the symmetrical plane at a bench height of 24 m, a length of 20 m, and a width of 15 m. The designed batter angle was 75°. ANSYS was used for simulation work via a hexahedral mesh generated by Hypermesh 14.0. When defining the boundary conditions, the section (shot hole surface) of the model was considered as the symmetrical boundary, and the other surfaces except the section are all nonprojection boundaries. The crest, surface, and toe of the batter were set as free face, as shown in Figure 2.

Three sets of numerical models were established based on the figure to represent the field conditions. Dynamic loading and rock yield time were quantitatively studied by using millisecond blasting while reasonably setting delay time, detonation sequence, and detonation location. A parametric study was also carried out on millisecond time of the digital electronic detonated. The detonation combinations can be seen in Table 1.

The dynamic experiments on many materials [23] show that the dynamic yield stress was significantly higher than the static yield stress. The Cowper-Symonds relationship is

Table 1: Simulation parameters of millisecond blasting in the hole.

	B-section delay time	3 ms				5 ms				7 ms			
Parameters of millisecond blasting	B & D combined detonation	1	2	3	4	5	6	7	8	9	10	11	12
		D top & B bottom		D top & B top	D bottom & B bottom	D top & B top	D top & B bottom	D bottom & B top	D bottom & B bottom	D top & B top	D top & B bottom	D bottom & B top	D bottom & B bottom
	D-section detonation location	0	0	0	0	0	0	0	0	0	0	0	0
		0.5	0.5	0.5	0.5	0.5	0.5	0.5	0.5	0.5	0.5	0.5	0.5
		1.0	1.0	1.0	1.0	1.0	1.0	1.0	1.0	1.0	1.0	1.0	1.0
		1.5	1.5	1.5	1.5	1.5	1.5	1.5	1.5	1.5	1.5	1.5	1.5

a simple empirical formula between the dynamic yield stress and strain rate ([24, 25]; [26]), which was proposed on the basis of a large number of experiments. This study investigated the feasibility of complete restart numerical simulation technology and the Lagrangian [27] numerical algorithm on multistage rock blasting simulation. The constitutive model of rock material was not studied in detail, such that a bilinear kinematic hardening model (plastic kinematic constitutive model) was used for rock material based on the Cowper-Symonds relationship [28]. This is a commonly used model for rock and soil simulation. The expression is as follows:

$$\sigma_Y = \left[1 + \left(\frac{\varepsilon *}{C}\right)^{1/P}\right]\left(\sigma_0 + \beta E_{\mathrm{P}} \cdot \varepsilon_{\mathrm{eff}}^{p}\right), \tag{17}$$

where σ_0 is the initial yield strength. C and P are constant related to material properties, $C = 35$ and $P = 3$. $\varepsilon *$ is strain rate, and $\beta = 1$ (adjustable parameter). E_{P} is the modulus of hardening (24 MPa), $\varepsilon^{\mathrm{P}}{}_{ij}$ is plastic strain rate, and $\varepsilon^{\mathrm{P}}{}_{\mathrm{eff}}$ is equivalent plastic strain, which can be calculated as $\varepsilon^{\mathrm{P}}{}_{\mathrm{eff}} = \int_0^t (2\varepsilon^{\mathrm{P}}{}_{ij}/3)^{1/2} dt$.

The elements of rock and blast hole filling were defined as "∗sect-lag"; and rock and stemming materials were assumed to be subject to the constant-stress solid element algorithm (see Tables 2 and 3 for details).

The element of the spaced air in the hole was defined as "∗sect-ale". Mat-Null material model (5) was used to represent air; and other parameters were set as default. The state equation of air is the ideal air equation (∗EOS-001). This equation is a linear polynomial, and the material parameters at initial state were defined using thermodynamics:

$$p = \frac{(\gamma - 1)\rho E}{\rho_{\mathrm{air}}}, \tag{18}$$

where γ is the adiabatic index (=1.4), $\rho_{\mathrm{air}} = 1.29$ g/L, ρ is the density at certain time, and E is the specific internal energy[29]. The JWL [24] equation was used for emulsion explosives, which can precisely describe the expansion process of detonation products. This equation has an extensive database for various explosives and is expressed as

Table 2: Blocking material parameters.

Density (g/cm^3)	Elastic modulus (GPa)	Poisson's ratio	Yield strength (MPa)	Tangent modulus (MPa)
1.85	1.2	0.38	0.8	0.1

Table 3: Dolomite material parameters.

Density (g/cm^3)	Elastic modulus (GPa)	Poisson's ratio	Tensile strength (MPa)	Compressive strength (MPa)
2.43	5	0.30	4	80

$$P = A\left[\frac{1-w}{R_1 V}\right]e^{-R_1 V} + B\left[\frac{1-w}{R_2 V}\right]e^{-R_2 V} + \frac{\mathrm{wE}}{V}, \tag{19}$$

where P is the required pressure and E is internal energy of detonation product per unit volume (assumed as 50 GPa). According to Min et al. in the literature [23, 30–32], ρ and v were obtained, respectively, at values of 1.2 g·cm^{-3} and 0.4 cm·μs^{-1}. V is volume of detonation product, $A = 2.14 \times 1011$, $B = 1.82 \times 109$, $R_1 = 4.15$, $R_2 = 0.95$, and $w = 0.5$.

3.1. Determination of Detonation Location and Combination. Detonation location was investigated first while keeping other parameters the same. Although simultaneous initiation method is the most efficient way for rock fragmentation, it is difficult to be achieved due to clamping effect of the lower rock. Intermediate initiation and two-end initiation methods within the hole are more effective than bottom-end initiation method considering the length of the charge from the deep-hole blasting and superposition of detonation waves. Based on the engineering practice, this paper simulated the single-point detonation with initiation point at the bottom of the hole. This section discusses the change of the effective stress in the intermediate air interval at various millisecond time intervals (3-8 ms). Rock strengths at Barun Mine were obtained by conducting laboratory experiments on the rock specimen collected from the toe of 1548 slope, at an average uniaxial compressive strength of 35 MPa and ultimate tensile strength of 4 MPa. The average tensile strength was used as the critical value of the failure criterion. In other words, the colored area

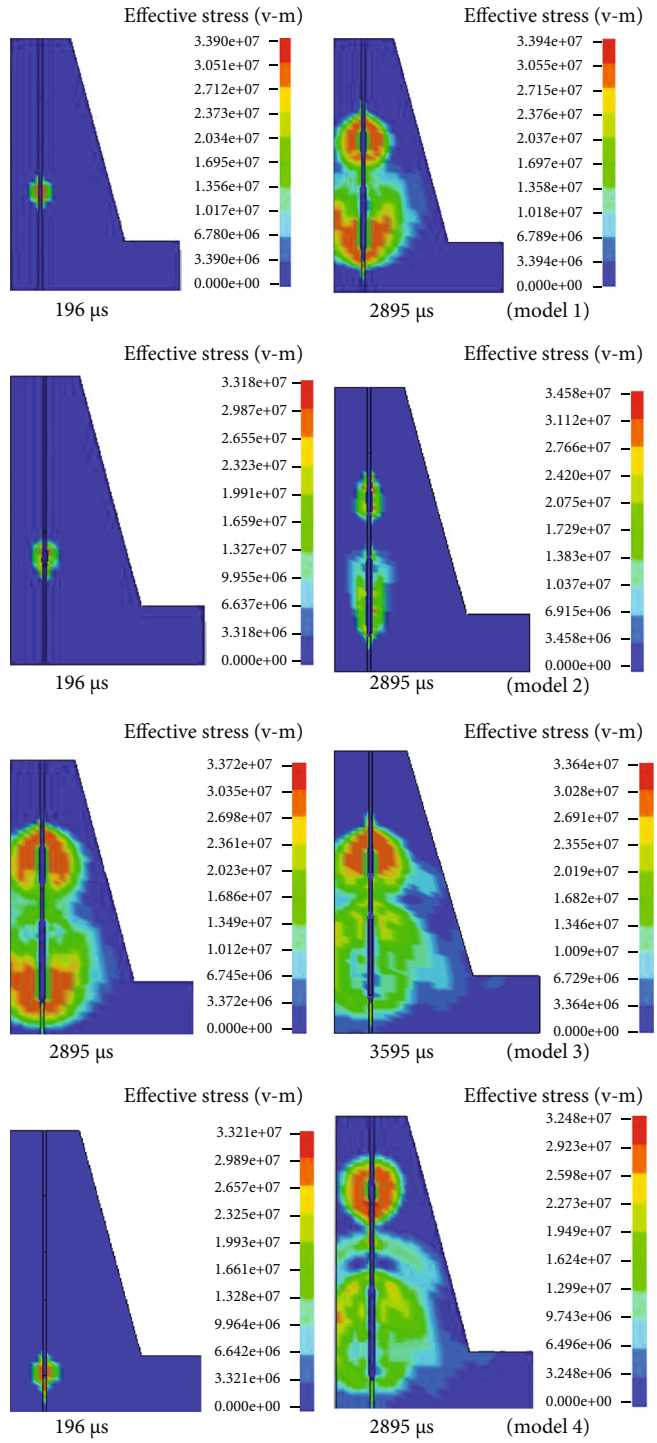

Figure 3: Equivalent stress cloud at different times.

under the stress of the rock mass corresponding to the blast hole is in a critical or plastic strain state.

Figure 3 shows the changes in the Mises stress cloud diagram of high-bench blasting at various conditions. The explosives at the bottom of the blasting hole detonated first, and the detonation wave propagated from bottom to top. By then, the stress wave extended outward in a "teardrop-shape" in the rock mass. The stress subsequently decreased as decaying of detonation wave energy. When $t = 2199\,\mu s$ in model 3, the bottom 8 m explosives were detonated first and the stress wave of the bottom explosive began to propagate in the 5 m air interval while the upper explosives were set to detonate 3 ms later. Since then, part of detonation wave from upper explosives propagated towards the surface, whereas the other parts started to propagate downwards along the upper 6 m explosives. When $t = 2895\,\mu s$, the stress

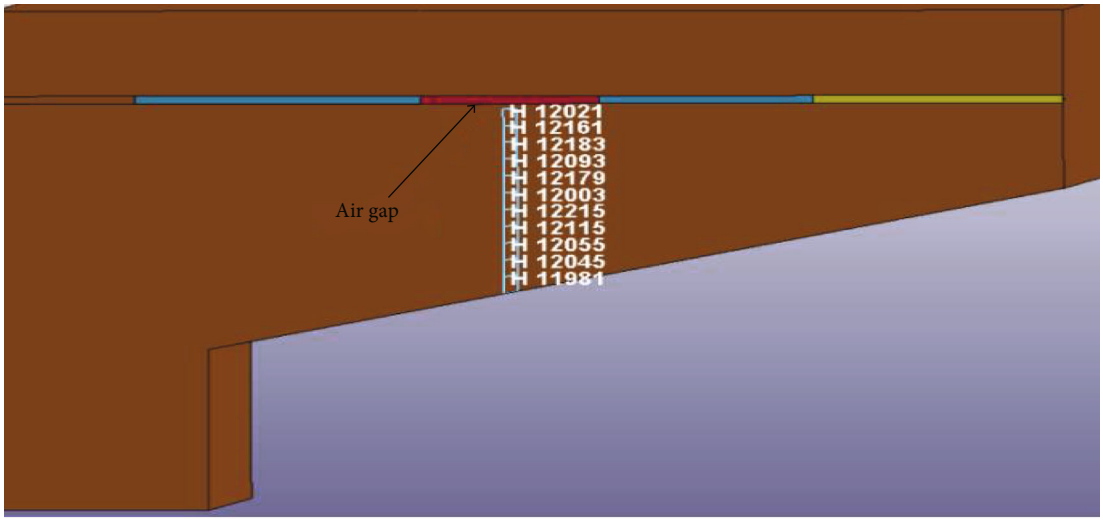

Figure 4: Locations of equidistant monitoring points in the air compartment.

waves of the upper and lower explosives collided and superimposed. At this point, the bottom explosives that detonated first completed full detonation. The decaying stress area started to increase and expand again. Subsequently, it propagated until the delaying of the stress area was less than the yield strength of the rock mass; and the whole explosion process was completed. The changes in the Mises stress cloud diagram of high-bench blasting at different times in model 3 show that the detonation wave superimposition of the upper and lower explosives induced stress superposition. This resulted in the stress decay rate in the rock body slower than the previous period. At this stage, the air interval in the blasting hole played a critical role in prolonging the detonation time such that the rock was subjected to a longer lasting stress. This in turn achieved an ideal rock breaking effect. Results from other models are similar to those shown in model 3, such that they are not discussed here.

The delayed detonation in the high step hole adopts air interval detonation. This is because the air had lower resistance to the rock mass, such that the explosion energy of the upper and lower sections can be directed to intermediate section first, which can effectively store energy while prolonging the effective time of detonation air. Thereby, this part of the corresponding rock mass was far away from the explosive energy, so that the explosion stress distribution was relatively small.

Therefore, the equidistant interval was used in the intermediate air interval to determine monitoring point locations H12021~H11981, as shown in Figure 4. The stress curve of different monitoring units was calculated by the LS-prepost postprocessor; and the peak effective stress in each unit was obtained. By then, the trend of Miss stress in the units during blasting was obtained from the model.

Based on the field experience and combination of initiation methods, the initiation position was determined to be 0.5 m from the bottom explosives and gradually increased the bottom initiation position by every 0.5 m. In this simulation, the bottom initiation positions were selected as 0.0 m, 0.5 m, 1.0 m, and 1.5 m from the hole base. According to the stress time curve diagram of each point, the peak value of the overall waveforms under all cases rose first and then decreased with increasing time, although the time interval when the peak stress was over rock strength was different for each case. As the distance between the monitoring point and the air column increases, the rate of stress reduction at the monitoring point, that is, the degree of flatness of the curve, was different. Schemes 4-1 and 4-2 have steeper slopes than the curves of 3-1 and 3-2.

As there are variations during numerical calibration, Scheme 3.2 had most fluctuation with a range between 0.2 MPa and 0.4 MPa; this variation was within the tolerant level. The other curves were relatively flat, and the curve in Scheme 4-1 had the flattest slope. The flatness of the curve reflected the uniformity of the explosion energy distribution, such that Scheme 4.1 had the most uniformed explosion energy distribution. This was a more effective utilization of explosion energy. At 1 m initiation position, the peak effective stress of the element was greater than the dynamic tensile strength of the rock, which means the element had yielded and "flaking" had occurred. If one unit does not yield, it can be considered that the blasting process produced a large block (>1 m) than since the distance between the selected units was 1.0 m. It is very likely that the blasting plan should be improved based on the parameters of the mining equipment. From Scheme 4-1 in Figure 5, it can be seen that all units yielded; while the peak effective stresses of some units in Scheme 3.1 were lower than the dynamic tensile strength of the rock, which may result in larger blocks.

Based on the field experience at Barun Mine and the authors' experience on millisecond blasting, the initiation time of the upper and lower charges in the hole was set between 3 ms and 8 ms delay time.

With different initiation parameters, the bottom initiation distance was set as 0 m, 0.5 m, 1.0 m, and 1.5 m. Results showed that under Schemes 3-1, 3-2, 4-1, and 4-2, the average peak effective stresses are at the monitoring points (see

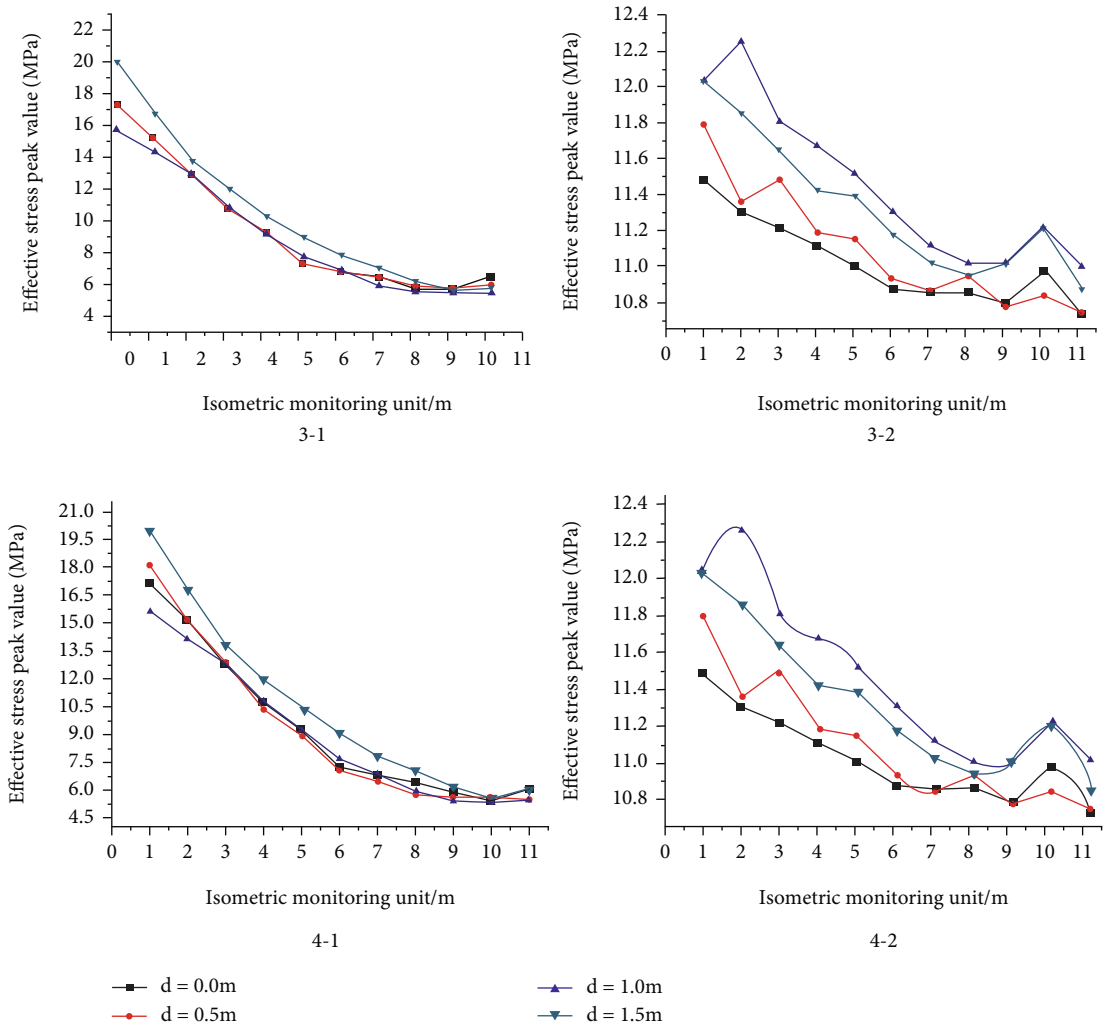

(a) 3 ms

Figure 5: Continued.

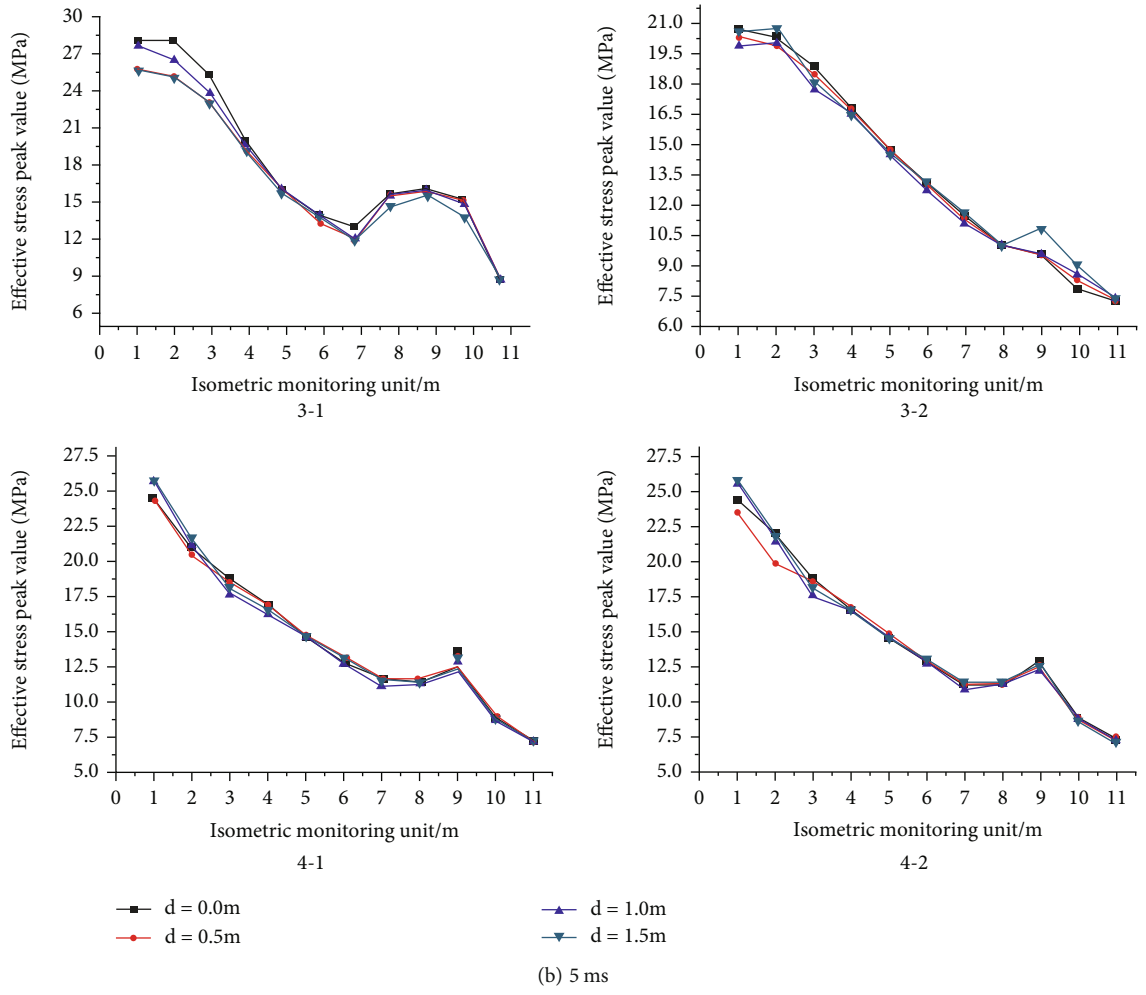

(b) 5 ms

Figure 5: Continued.

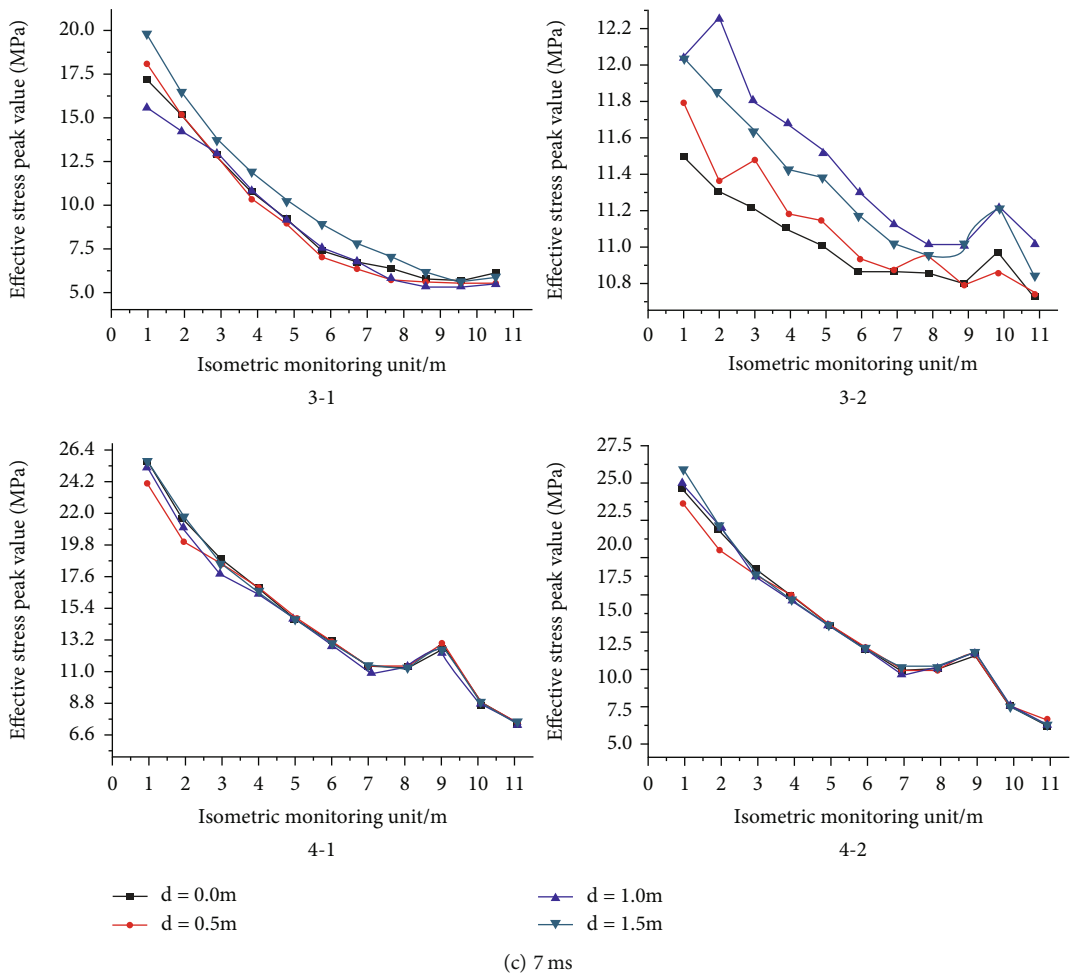

(c) 7 ms

Figure 5: Peak effective stress diagram at equidistant monitoring points of interval air column.

Table 4: Peak effective stress of the inspection points under the millisecond blasting.

Initiation method	Peak effective stress (MPa)				
	Initiation location 0 m	0.5 m	1.0 m	1.5 m	Difference between maximum and minimum
3-1	9.37	9.25	9.05	10.36	1.31
3-2	10.02	10.09	14.50	13.23	4.48
4-1	15.80	15.40	15.55	15.46	0.40
4-2	14.38	14.14	14.18	14.45	0.07
Difference between maximum and minimum	6.43	6.15	6.50	5.10	///

Table 4 for details). It also shows that under the same bottom detonation distance, the detonation method had an impact on the peak effective stress at each monitoring point, with a variation between 5.10 and 6.50 MPa. On the contrary, under the same detonation method and different bottom detonation distances, the peak effective stress of each monitoring unit varied from 0.07 MPa to 4.48 MPa, while the millisecond initiation sequence influenced the fragmentation and was larger than the bottom initiation distance. Considering the changes in the peak effective stress values at each point around the intermediate air space, the intensity of the full stress field, and the duration, the best millisecond initiation parameter was determined, i.e. millisecond time of 3~8 ms. Based on model 3, the initiation distance was determined to be 1 m.

3.2. Field Test. Barun Mine is a subsidiary of Baotou Iron and Steel Group. The main drilling equipment of Barun Mine is a KY-310 roller drilling rig. The prestrip equipment mainly includes ER9350 large hydraulic shovel Liebherr and 4410 large electric truck. It is a modern superpit. The lithology at the site is mainly dolomite, slate, and Quaternary. Due to the requirement of pit boundary optimization, the highwall needs to be expanded towards the north. To improve the efficiency of the expansion, Barun Mine decided to utilize the upper existing 12 m high bench, modification of

Figure 6: Rock fragmentation at front of high-bench blasting.

Figure 7: Rock fragmentation at the crest of high-bench blasting.

drilling rig, and production process. The upper 12 m bench was expanded to a 24 m high bench without the change of original mine design parameters. Thus, 24 m boreholes through two benches were drilled at one time. This would increase the efficiency of blasting. Due to the height of the benches at Barun Mine, the factors including blast reliability improvement were considered; such improvement was achieved by setting initiation points at top and bottom of the blasting hole. However, with the increase in bench height, the length of the explosives in the blasting hole also decreased. It was required to redetermine the parameters of explosives in the upper and lower segments of the blast hole.

The blasting zone was located on the north side of the pit at the level of 1548. The bench lithology is mainly medium strength dolomite. Blasting holes had a diameter of 310 mm and a chassis resistance line of 10 m. To reduce the influence of blasting vibration, the short delay time in the holes was set as 3~8 ms and the detonation was carried out between the rows. The charging method was interval charging with 7 m stemming. There were 71 blast holes in total, and the rock blasting volume was 66 134.88 t. Based on the field test results, it can be seen that the average block size satisfied the requirements of shoveling. The block diameter was about 20 cm, and the forward moving was about 20 m. The back and side movements were limited by other in-rock masses, such that the distance was relatively small, at approximately 3 m. The reasonable fragmentation size was acceptable and uniform, which satisfied the capacity of mining equipment. The throwing distance of the blasted rock was greater than 25 m. The on-site blasting results are shown in Figures 6 and 7.

4. Conclusion

Under the condition of 24 m bench and large vertical drilling at Barun Mine, multiple analytical and numerical models were constructed to analyze the distribution of blasting stress in the rock mass at various initiation sequence and locations. The millisecond blasting initiation parameters provided a theoretical basis for high-bench blasting; and the following conclusions were drawn:

(1) Based on numerical simulation and field test, it was concluded that the effective stress duration was longer when the lower end of the lower explosives was detonated first and the millisecond time interval between

the holes is 3~8 ms. The delayed detonation at the top of the upper grain is reasonable, which can result in sufficient rock fragmentation. This provided a favorable analysis and technical support for the development of the millisecond blasting at Barun Mine

(2) By comparing the peak stresses of same detonation sequence under different detonation locations with the same detonation location under different detonation sequences, it was found that the millisecond initiation sequence was the key factor affecting the rock fragmentation. Thereby, the emerging high-precision digital electronic detonators provide sufficient preciseness for millisecond blasting in high-bench holes. Moving forward, the advantages of electronic detonators will be further utilized to specific working conditions, aiming at improving the blasting efficiency of open-cut operations

List of Symbols

a: Interval of explosive packs, m
C and P: Constant related to material properties, $C = 35$ and $P = 3$
E_p: Modulus of hardening, MPa
E: Internal energy of detonation product per unit volume, GPa
F: Function
ΔP_t: Change of shock wave peak overpressure over time, MPa
ΔP_f: Peak shock wave overpressure, MPa
P: The required pressure, MPa
p_{vp}: Pressure of exploded air, MPa
$*p_w$: Average detonation pressure of exploded air, MPa
R_w: Radius of detonation wave front, m
R_{vp}: Radius of the exploded air, m
R_{vd}: Blasting cavity radius, m
R_w: Radius of concentrated charge pack, m
R: The distance between blasting center to the measurement point, m
s: Crack width
t_p: Duration of shock wave overexposure, ms
t: Time, ms
t_1: Barotropic pressure, MPa
t_2: Millisecond time, ms
u_{tr}: Speed of crack propagation
u_r: Average speed of flying rock
W: Weight of emulsion explosive, kg
Z: Proportional explosion distance, m/kg$^{1/3}$
ρ_0: Initial density, kg/m^3
ρ_1: Density at any moment, kg/m^3
ρ_w: Explosive density, kg/m^3
α_0: Attenuation coefficient
c_p: Speed of longitudinal wave in the medium, m/s
σ_0: Initial yield strength
$\varepsilon *$: Strain rate
β: 1 (adjustable parameter)
$\varepsilon^p{}_{ij}$: Plastic strain rate
$\varepsilon^p{}_{eff}$: Equivalent plastic strain.

Data Availability

The data basically comes from the mining data of the Baiyun Obo rare earth mine. This article makes a corresponding study on the delay time in the hole.

Additional Points

Highlights. The delayed detonation at the top of the upper grain is reasonable, which can result in sufficient rock fragmentation. This provided a favorable analysis and technical support for the development of the millisecond blasting at Barun Mine. The emerging high-precision digital electronic detonators provide sufficient preciseness for millisecond blasting in high-bench holes. Moving forward, the advantages of electronic detonators will be further utilized to specific working conditions, aiming at improving the blasting efficiency of open-cut operations

Conflicts of Interest

The authors declared that they have no conflicts of interest in this work.

Acknowledgments

The work of this paper is supported by the Research and application of 24 m high step expansion blasting technology in Baiyun Eboxi Mine.

References

[1] L. Zhendong, F. Yong, and W. Lu, "Analysis of explosion energy transmission and rock breaking effect under dual-point initiation in a hole," *Chinese Journal of Rock Mechanics and Engineering*, vol. 38, pp. 1–13, 2019.

[2] G. Qidong, L. Wenbo, and L. Zhendong, "Study on the control effect of the initiation position in the hole on the energy transmission of the explosion in rock blasting," *Chinese Journal of Geotechnical Engineering*, vol. 42, no. 11, pp. 2050–2058, 2021.

[3] L. Wu, L. Hongwei, and N. Huajun, "Experimental study on the influence of millisecond delay time on rock breaking effect," *Pyrotechnics*, vol. 8, no. 4, pp. 52–57, 2020.

[4] C. Shihai, S. Hu, and C. Shaofeng, "Study on the influence of millisecond time and cylindrical charge characteristics on blasting vibration effect," *Chinese Journal of Rock Mechanics and Engineering*, vol. 36, no. S2, pp. 3974–3983, 2017.

[5] Y. Zhongwen, Z. Shichun, and Q. Peng, "Crack propagation mechanism of short-delay blasting in slit charge bag," *Journal of China Coal Society*, vol. 43, no. 3, pp. 638–645, 2018.

[6] Z. Sherong, L. Hongbi, and G. Wang, "Comparative analysis of grid size effects in numerical simulation of air and underwater explosion shock waves," *Journal of Hydraulic Engineering*, vol. 46, no. 3, pp. 298–306, 2015.

[7] H. Liangliang, H. Ruiyuan, and L. Shichao, "Numerical simulation study of underwater explosion shock wave," *Chinese Journal of High Pressure Physics*, vol. 34, no. 1, pp. 1–13, 2020.

[8] X. Xie, "Development status and prospect of fine blasting," *Engineering Science of China*, vol. 16, no. 11, pp. 14–19, 2014.

[9] G. Deyong, Z. Chao, and Z. Tonggong, "The influence of the initiation position of deep-hole shaped energy blasting on coal

seam fracturing and anti-reflection," *Journal of China Coal Society*, vol. 1078, 2020.

[10] L. Zhendong, W. Lu, and F. Yong, "Explosion energy distribution under lateral initiation conditions and its influence on rock breaking effect," *Explosion and Shock*, vol. 37, no. 4, pp. 661–670, 2017.

[11] L. Qiyue and L. Xiuquan, "The construction method of ANSYS three-dimensional complex model based on SURPAC," *Mining and Metallurgical Engine*, vol. 34, no. 5, pp. 1–5, 2014.

[12] L. Tong, C. Ming, and Y. Zhiwei, "Research on the energy transfer efficiency of blasting explosion with different coupling media," *Explosion and Shock*, vol. 41, no. 6, pp. 1–13, 2021.

[13] W. Dong, C. Ming, and Y. Zhiwei, "Research on the blasting damage area of rock mass based on the dynamic characteristics of strain rate," *Engineering Science and Technology*, vol. 53, no. 1, pp. 67–74, 2021.

[14] J. Henry and X. Jianguo, *Explosive Dynamics and Its Applications*, Science Press, Beijing, 1981.

[15] S. Wu, J. Li, J. Guo, G. Shi, Q. Gu, and C. Lu, "Stress corrosion cracking fracture mechanism of cold-drawn high-carbon cable bolts," *Materials Science and Engineering: A*, vol. 769, pp. 1–10, 2020.

[16] S. Wu, H. L. Ramandi, H. Chen, A. Crosky, P. Hagan, and S. Saydam, "Mineralogically influenced stress corrosion cracking of rockbolts and cable bolts in underground mines," *International Journal of Rock Mechanics and Mining Sciences*, vol. 119, pp. 109–116, 2019.

[17] S. Wu, X. Zhang, J. Li, and Z. Wang, "Investigation for influences of seepage on mechanical properties of rocks using acoustic emission technique," *Geofluids*, vol. 2020, Article ID 6693920, 10 pages, 2020.

[18] Q. Qihu, "Several progress in rock explosion dynamics," *Chinese Journal of Rock Mechanics and Engineering*, vol. 28, no. 10, pp. 1945–1968, 2009.

[19] L. Xiaoming, Z. Wenhai, and J. Wenbin, "Optimal delay control of millisecond blasting for rock breaking mechanism," *Journal of Harbin Institute of Technology*, vol. 49, no. 2, pp. 158–163, 2017.

[20] L. Zhendong, W. Lu, and H. Hu, "The influence of blasting free surface on the peak of vibration induced by millisecond blasting on slope," *Chinese Journal of Rock Mechanics and Engineering*, vol. 35, no. 9, pp. 1815–1822, 2016.

[21] Z. Wenhai, *Selection of hole-by-hole initiation delay time for deep-hole bench blasting in open-pit mine*, Fuzhou University, 2015.

[22] S. Jianfeng, Z. Dongwang, and H. Xiaowu, "Model test study on the best time delay between drilling and blasting holes," *Metal Mine*, vol. 6, pp. 19–22, 2015.

[23] C. Yu, L. Liangzhong, and H. Yimin, "Study on the detonation product of aluminum-containing explosives JWL equation of state," *Explosion and Shock*, vol. 19, no. 3, pp. 274–279, 1999.

[24] R. Yang, D. Chenxi, and G. Yang, "Experimental study on crack propagation characteristics of milli second blasting," *Explosion and Shock Wave*, vol. 36, no. 24, pp. 98–103, 2017.

[25] Z. Wenjun, N. Hongxin, and S. Wang, "Optimization of preprocessing for engineering blasting simulation based on HyperMesh," *Computer Aided Engineering*, vol. 29, no. 4, pp. 50–56, 2020.

[26] Q. Gao, W. Lu, and L. Zhendong, "Research on the control effect of the initiation position in the hole on the energy transmission of the explosion in rock blasting," *Chinese Journal of Rock Engineering*, vol. 42, no. 11, pp. 2050–2059, 2020.

[27] R. Cai, Y. Li, C. Zhang et al., "Damage assessment of prefabricated prestressed channel slab under plane charge blast," *Journal Engineering Structures*, vol. 246, p. 113021, 2021.

[28] J. Chen, Y. Zhao, H. Zhao, J. Zhang, C. Zhang, and D. Li, "Analytic study on the force transfer of full encapsulating rockbolts subjected to tensile force," *International Journal of Applied Mechanics*, vol. 13, no. 9, 2021.

[29] Q. He, L. Zhu, and L. Yingchun, *Simulating hydraulic fracture re-orientation from oriented perforations in heterogeneous rocks with an improved discrete element method*, Rock Mechanics and Rock Engineering, 2021.

[30] G. Min, W. Canhua, and L. L. Xun, "Determination and function of main blasting parameters in hard rock excavation," *Journal of China Coal Society*, vol. 40, no. 7, pp. 1526–1533, 2015.

[31] J. Chen, P. Liu, H. Zhao, C. Zhang, and J. Zhang, "Analytical studying the axial performance of fully encapsulated rock bolts," *Engineering Failure Analysis*, vol. 128, p. 105580, 2021.

[32] J. Chen, H. Zhao, F. He, J. Zhang, and K. Tao, "Studying the performance of fully encapsulated rock bolts with modified structural elements," *International Journal of Coal Science and Technology*, vol. 8, no. 1, pp. 64–76, 2021.